








## Article

# Electrooxidation of Urea in Alkaline Solution Using Nickel Hydroxide Activated Carbon Paper Electrodeposited from DMSO Solution

Saba A. Aladeemy <sup>1,2</sup> , Abdullah M. Al-Mayouf <sup>1,2,\*</sup> , Maged N. Shaddad <sup>1</sup> , Mabrook S. Amer <sup>2</sup> ,  
Nawier K. Almutairi <sup>1</sup>, Mohamed A. Ghanem <sup>1</sup> , Nouf H. Alotaibi <sup>1</sup>  and Prabhakarn Arunachalam <sup>1,\*</sup> 

<sup>1</sup> Electrochemistry Sciences Research Chair (ESRC), Department of Chemistry, Science College, King Saud University, Riyadh 11451, Saudi Arabia; sabaameen98@yahoo.com (S.A.A.); mshaddad@ksu.edu.sa (M.N.S.); noiralmtiri70008@gmail.com (N.K.A.); mghanem@ksu.edu.sa (M.A.G.); nhalotaibi@ksu.edu.sa (N.H.A.)  
<sup>2</sup> K.A.CARE Energy Research and Innovation Center, Riyadh 11454, Saudi Arabia; msamer@ksu.edu.sa  
\* Correspondence: amayouf@ksu.edu.sa (A.M.A.-M.); parunachalam@ksu.edu.sa (P.A.); Tel.: +966-114-696-026 (P.A.)

**Abstract:** Electrooxidation of urea plays a substantial role in the elimination of urea-containing wastewater and industrial urea. Here, we report the electrodeposition of nickel hydroxide catalyst on commercial carbon paper (CP) electrodes from dimethyl sulphoxide solvent (Ni(OH)<sub>2</sub>-DMSO/CP) for urea electrooxidation under alkaline conditions. The physicochemical features of Ni(OH)<sub>2</sub>-DMSO/CP catalysts using scanning electron microscopy and X-ray photoelectron spectroscopy revealed that the Ni(OH)<sub>2</sub>-DMSO/CP catalyst shows nanoparticle features, with loading of <1 wt%. The cyclic voltammetry and electrochemical impedance spectroscopy revealed that the Ni(OH)<sub>2</sub>-DMSO/CP electrode has a urea oxidation onset potential of 0.33 V vs. Ag/AgCl and superior electrocatalytic performance, which is a more than 2-fold higher activity in comparison with the counterpart Ni(OH)<sub>2</sub> catalyst prepared from the aqueous electrolyte. As expected, the enhancement in electrocatalytic activity towards urea was associated with the superficial enrichment in the electrochemically active surface area of the Ni(OH)<sub>2</sub>-DMSO/CP electrodes. The results might be a promising way to activate commercial carbon paper with efficient transition metal electrocatalysts, for urea electrooxidation uses in sustainable energy systems, and for relieving water contamination.

**Keywords:** nickel hydroxide; non-aqueous solvents; electrooxidation; electrodeposition; urea



**Citation:** Aladeemy, S.A.; Al-Mayouf, A.M.; Shaddad, M.N.; Amer, M.S.; Almutairi, N.K.; Ghanem, M.A.; Alotaibi, N.H.; Arunachalam, P. Electrooxidation of Urea in Alkaline Solution Using Nickel Hydroxide Activated Carbon Paper Electrodeposited from DMSO Solution. *Catalysts* **2021**, *11*, 102. <https://doi.org/10.3390/catal11010102>

Received: 24 November 2020

Accepted: 8 January 2021

Published: 13 January 2021

**Publisher's Note:** MDPI stays neutral with regard to jurisdictional claims in published maps and institutional affiliations.



**Copyright:** © 2021 by the authors. Licensee MDPI, Basel, Switzerland. This article is an open access article distributed under the terms and conditions of the Creative Commons Attribution (CC BY) license (<https://creativecommons.org/licenses/by/4.0/>).

## 1. Introduction

The global increase in energy requirements has directed the search for alternate clean energy resources other than fossil fuels. Substantial interest has been focused on producing hydrogen (H<sub>2</sub>) from wastewaters and reducing greenhouse gas emissions (e.g., carbon dioxide) due to environmental concerns [1]. An organic carbamide, urea has been recognized as an appropriate hydrogen storage medium for long-standing, sustainable energy sources. This is due to its comparatively non-toxic, non-combustible, easy handling, storage-stable, and renewable features [2,3]. Besides, urea-containing wastewater is created abundantly from human/animal excretion and urea's industrial production [4,5]. The amount of urea and its compounds in our environment, particularly in groundwater, is increasing. The natural decomposition products of urea, such as nitrate and toxic ammonia, lead to environmental pollution and human health issues [6]. The available de-nitrification methodology is very expensive and inefficient, and hence a more proficient technology should be developed. Electrocatalytic action for urea-containing wastewater has been receiving substantial consideration due to its potential uses, including wastewater treatment, H<sub>2</sub> production, biosensors, and fuel cells [7–10]. The electrochemical urea oxidation reaction (UOR) directly converts urea to the value-added product of H<sub>2</sub>, or produces electricity at the cathode via fuel cell-based urea [11–13]. Notably, Boggs et al.

have summarized the energy consumption parameters and economic cost requirements for hydrogen production from water and urea electrolysis. Theoretically,  $H_2$  can be produced at the cost of \$0.69/kg based on an electricity cost of \$0.07 kW/h [4]. These methods offer an efficient way to sustainably alleviate water pollution, and provide alternative energy sources.

Numerous precious metal-containing electrocatalysts have been applied for UOR [4,14–16]. In recent years, cost-effective electrocatalysts, including nickel-containing electrodes, have been recommended as an active and durable catalyst for the electrooxidation of smaller organic materials [17,18] and for UOR under alkaline conditions [19–21]. UOR is a complex process, requiring six electrons to perform the electrochemical reactions, as discussed in earlier reports [22–25]. For nickel electrodes in alkaline conditions, UORs obey the mechanistic catalyst restoration process, in which divalent  $Ni(OH)_2$  is electrooxidized to trivalent nickel oxyhydroxide ( $NiOOH$ ), whereby it catalyzes the reaction. More significantly, under standard circumstances, the UOR theoretical voltage (0.37 V) is substantially less than (1.23 V) mandatory for water electrolysis reaction. Hence, using UORs, nearly 70% cheaper  $H_2$  can be manufactured than other wastewater management, and additional  $H_2$  gas can be obtained at the cathode [26]. However, this reaction's sluggish kinetics have restricted its utilization to produce  $H_2$  gas [27–30]. Moreover, despite the Ni-based electrocatalysts' generally poor performance, UORs' features, stabilities, and over-potential are quite high (greater than 0.9 V) [31–35]. In this regard, Ni-based electrodes can drive the oxygen evolution reaction (OER) [36], whose influence as a competitive process further reduces the selectivity toward UORs. Therefore, obtaining abundant efficient, robust, and inexpensive electrocatalysts provides a chance of overcoming these challenges by reducing the over-potential and improving the efficiency of UORs.

At present, there are numerous methods applied to the synthesis of nickel-based electrodes, such as the sol-gel method [37], hydro/solvothermal method [38–40], microwave-assisted synthesis [41], and electrodeposition process [42–44]. More importantly, the electrodeposition approach has been recognized as a simple, high purity, and cost-effective technique for the commercial production of electrocatalysts. It represents one of the oldest surface engineering processes to make thin films, especially metals and their alloys, with various nanostructures, by controlling electrodeposition parameters [45–47]. In recent years, considerable research works have been performed on the nickel oxide/hydroxides methods of  $Ni(OH)_2$  nanoribbons [48], Ni-carbon sponge [44],  $Ni(OH)_2$  NS/carbon cloth [23], and  $\beta$ - $Ni(OH)_2$ -CNTs [49] catalysts for electrocatalytic UORs. In this context, our understanding of the role of  $Ni(OH)_2$  at the center of the reaction is still inadequate.

As a substitute for aqueous media, electrochemical deposition in an organic solution can address the water electrolysis and poor solubility issues [50–52]. Conversely, the electrodeposition of Ni in organic media has been successfully demonstrated to fabricate high-quality microstructures. Due to the organic media in electrodeposition, there is only one phase on the films deprived of additional phases. In addition, numerous attempts have been made at electrochemical growth of metal oxide thin films through dimethyl sulfoxide (DMSO) solvent and acquiring a high-quality microstructure with good adhesion, containing only one phase [52–55]. There have been no significant efforts to focus on the fabrication of electrodeposited nickel using DMSO solvent and to employ them as electrocatalysts for UORs. Thus, this examination will offer valuable details on the activation of commercial carbon paper (CP) electrodes for the electrocatalytic enhancement of UORs via a nickel-based catalyst.

Herein, nickel hydroxide ( $Ni(OH)_2$ ) electrodes were obtained via facile electrodeposition from two different solutions of non-aqueous (DMSO) and an aqueous solution of deionized water ( $H_2O$ ) on a commercial CP electrode for application of UORs in alkaline media. The morphological nature and surface element compositions were examined through various physicochemical characterization techniques. Under alkaline conditions, the comparative electrochemical activity of the non-aqueous electrodeposited  $Ni(OH)_2$ -

DMSO/CP catalysts for UORs were examined and compared to Ni-electrodes deposited from the aqueous solution.

## 2. Results and Discussion

### 2.1. Catalysts Characterization

In general, the electrodeposition of metal electrodes is carried out in an aqueous medium. In this context, metal coatings obtained through an aqueous medium might have hydrogen, which is observed to cause higher internal stress and cracks in the coated films, and which undesirably upsets the mechanical features of the coatings [56]. The other setbacks of electrodes obtained via the electrodeposition approach in aqueous media are the poor solubility, and that they readily undergo a hydrolysis process [57]. Furthermore, numerous side effects may influence the quality of the coating surfaces. The liberation of  $H_2$  molecules during the electrodeposition of metals in aqueous electrolytes might also create pinholes in the electrodeposits. Consequently, the hunt for other electrolytes for metal electrodeposition is of major significance. In this context, non-aqueous solutions with organic solvents, such as DMSO, might be employed.

Figure 1 demonstrates the preparation approach of the  $Ni(OH)_2$ -DMSO/CP electrodes. For the electrodeposited  $Ni(OH)_2$ -DW/CP electrodes in an aqueous medium, the fabricated deposited materials contained hydrogen, resulting in numerous holes over the electrode's surface; these significantly guided the binding force between the metal deposition and the CP support. In contrast, in an organic medium, DMSO molecules partly decayed during the electrochemical deposition process, and the decomposed products (perhaps dimethyl sulfide ( $CH_3-S-CH_3$ ) and sulfur molecules) were successively integrated into the catalyst, favoring  $Ni(OH)_2$ -grain refinement [58,59].

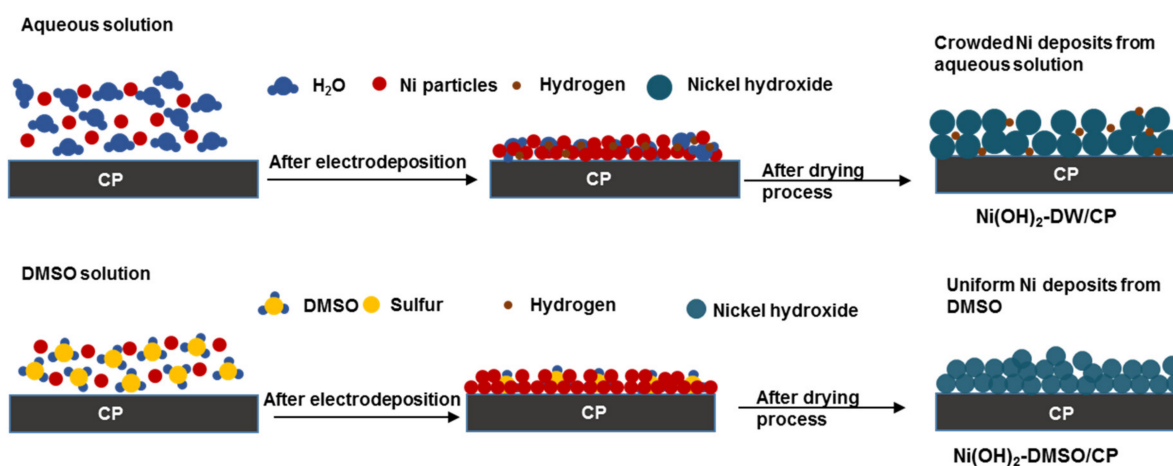


**Figure 1.** Schematic representation for the preparation of Nickel hydroxide electrodeposited on carbon paper under an aqueous and DMSO solution.

### 2.2. Morphological Characterization of Amorphous $Ni(OH)_2$

Electron microscopy measurements were applied to describe the fine structure and the morphological of the electrodeposited  $Ni(OH)_2$  electrocatalysts. Figure 2 displays the FE-SEM photographs of bare CP electrodes before, and after, the growth of  $Ni(OH)_2$  nanostructures prepared under different mediums, respectively. It can be evidenced that the CP was composed of aggregated carbon nanoparticles with a particle size ranging from 70–100 nm. The CP shows a greater surface area of  $100\text{ m}^2/\text{g}$  due to the interstitial mesoporous space between nanoparticles (Figure 2a). After the nickel was electrodeposited from the aqueous solution, the CP was fully covered by the  $Ni(OH)_2$  electrocatalyst, as presented in Figure 2b. The surface morphology in the FESEM image (Figure 2) clearly reveals the  $Ni(OH)_2$ -DW deposited from aqueous solution has an aggregated spherical 3D



nanoparticle morphology in the electrodeposit, and with random sizes. In contrast, the FESEM image in Figure 2c,d reveals that the  $\text{Ni}(\text{OH})_2$  electrodeposited from the DMSO ( $\text{Ni}(\text{OH})_2$ -DMSO/CP) resembles the morphology of a nanoparticle of CP substrate with the absence of the dense deposit that blocked the interstitial mesopore network, as in case of  $\text{Ni}(\text{OH})_2$ -DW catalysts. These  $\text{Ni}(\text{OH})_2$  particles over CP prepared from the DMSO solvent tend to have a superior specific surface area to an aqueous solution, and are anticipated to deliver more reactive sites for electrocatalytic reactions [60–62].

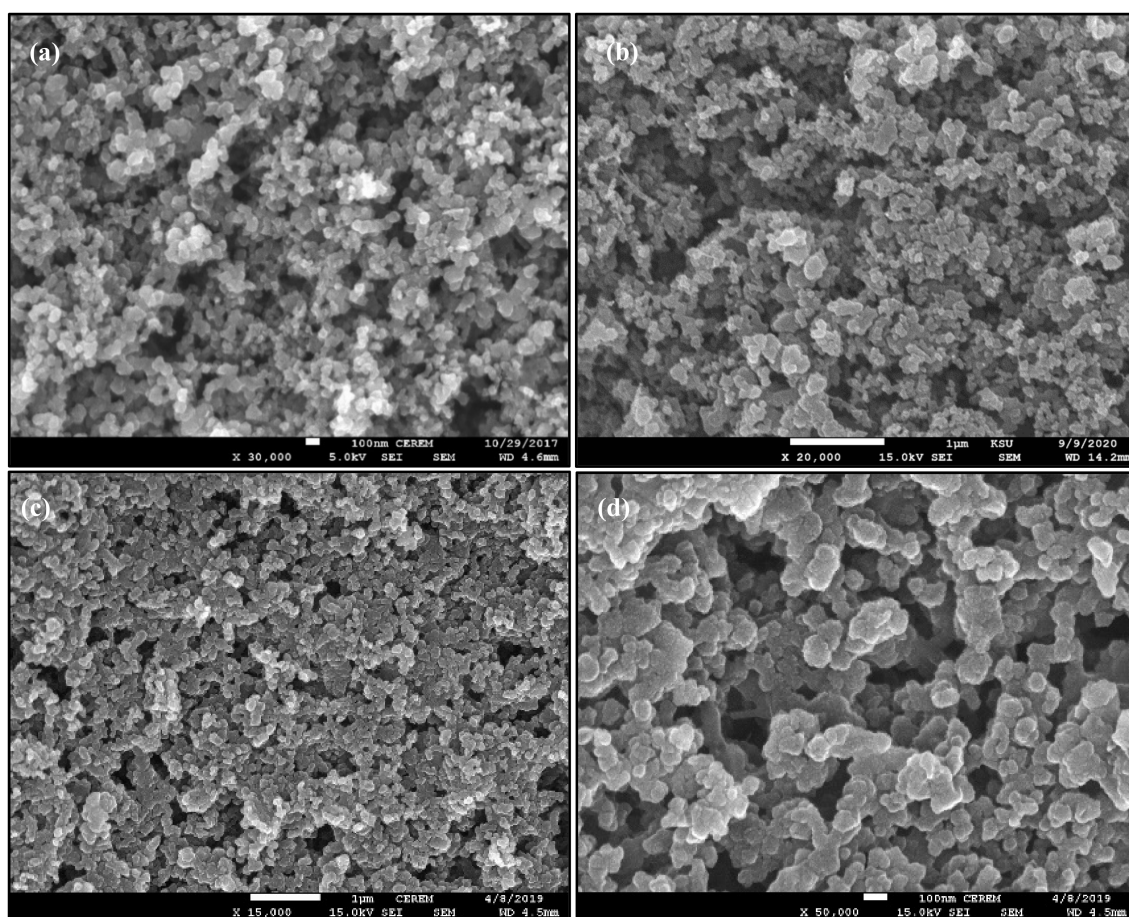


**Figure 2.** Morphological examination of  $\text{Ni}(\text{OH})_2$ /CP based electrodes prepared from two mediums. FE-SEM micrographs of CP (a),  $\text{Ni}(\text{OH})_2$ -deionized water (DW)/CP catalysts prepared under aqueous medium (b), and  $\text{Ni}(\text{OH})_2$ -dimethyl sulfoxide (DMSO)/CP electrodes (c,d) obtained through an electrodeposition approach through DMSO solution.

Supplementary Materials Figure S1 exhibits the TEM images of the  $\text{Ni}(\text{OH})_2$ -DW/CP and  $\text{Ni}(\text{OH})_2$ -DMSO/CP electrodes. The HRTEM image indicates  $\text{Ni}(\text{OH})_2$  nanoparticles distributed on the CP electrodes. Ni was detected in these nanoparticles by EDX (Supplementary Materials Figure S2). The C, O, and Cu signals were derived from the TEM grid with a supporting film. Supplementary Materials Figure S3 reveals the XRD of the fabricated  $\text{Ni}(\text{OH})_2$  supported on the CP substrate from an aqueous and DMSO medium. All the obtained diffraction peaks are indexed to the CP substrate. In addition, except for the peak related to the CP substrate, no peak of  $\text{Ni}(\text{OH})_2$  was present in the prepared electrode, which suggests the amorphous nature of the electrode.

### 2.3. Surface Features of $\text{Ni}(\text{OH})_2$ /CP

To obtain more evidence about the surface features of the  $\text{Ni}(\text{OH})_2$  catalysts over CP, Figure 3 displays the comparative XPS examination of the  $\text{Ni}(\text{OH})_2$ -DW/CP, and  $\text{Ni}(\text{OH})_2$ -DMSO/CP deposits. A representative survey of the XPS in Figure 3a discloses the



prominent photoelectron peaks, equivalent to Ni 2p and O 1s, which certified the presence of nickel and oxygen in the CP substrate. In the Ni(OH)<sub>2</sub>-DW/CP electrodes, Figure 3b displays the Ni 2p peak's deconvolution results, which reveal the spin-orbit doublets that agree with the 2p<sub>3/2</sub> and 2p<sub>1/2</sub> peaks were noticed at 855.4 and 873.06 eV. Moreover, a satellite peak for 2p<sub>3/2</sub> and 2p<sub>1/2</sub> was also identified at 861.1 and 878.5, correspondingly. The Ni 2p spectrum was also observed for Ni(OH)<sub>2</sub>-DW/CP deposits. Conversely, related to Ni(OH)<sub>2</sub>-DW/CP, all the Ni 2p peaks of Ni(OH)<sub>2</sub>-DMSO/CP were shifted markedly to higher binding energies. Furthermore, the spin-energy separation of the two prominent peaks was 17.7 eV, distinctive of Ni(OH)<sub>2</sub> phase [63]. Additionally, in the asymmetrical O 1s spectrum (Figure 3c), two prominent peaks, having binding energies of 530.4 and 531.7 eV, were noticed in the spectra of the Ni(OH)<sub>2</sub>-DW/CP deposit and were attributed to the lattice oxygen. However, the XPS of the O1S region of the Ni(OH)<sub>2</sub>-DMSO/CP deposit after disintegration split into three oxygen peaks, as displayed in Figure 3c. The fitted peak at 531.0 eV can be assigned to the Ni-O bonding [64], and the peak at 532.5 eV is attributed to the oxygen of hydroxyl groups [63]. Furthermore, the observed peak at 533.6 eV can be credited to surface adsorbed oxygen [65].

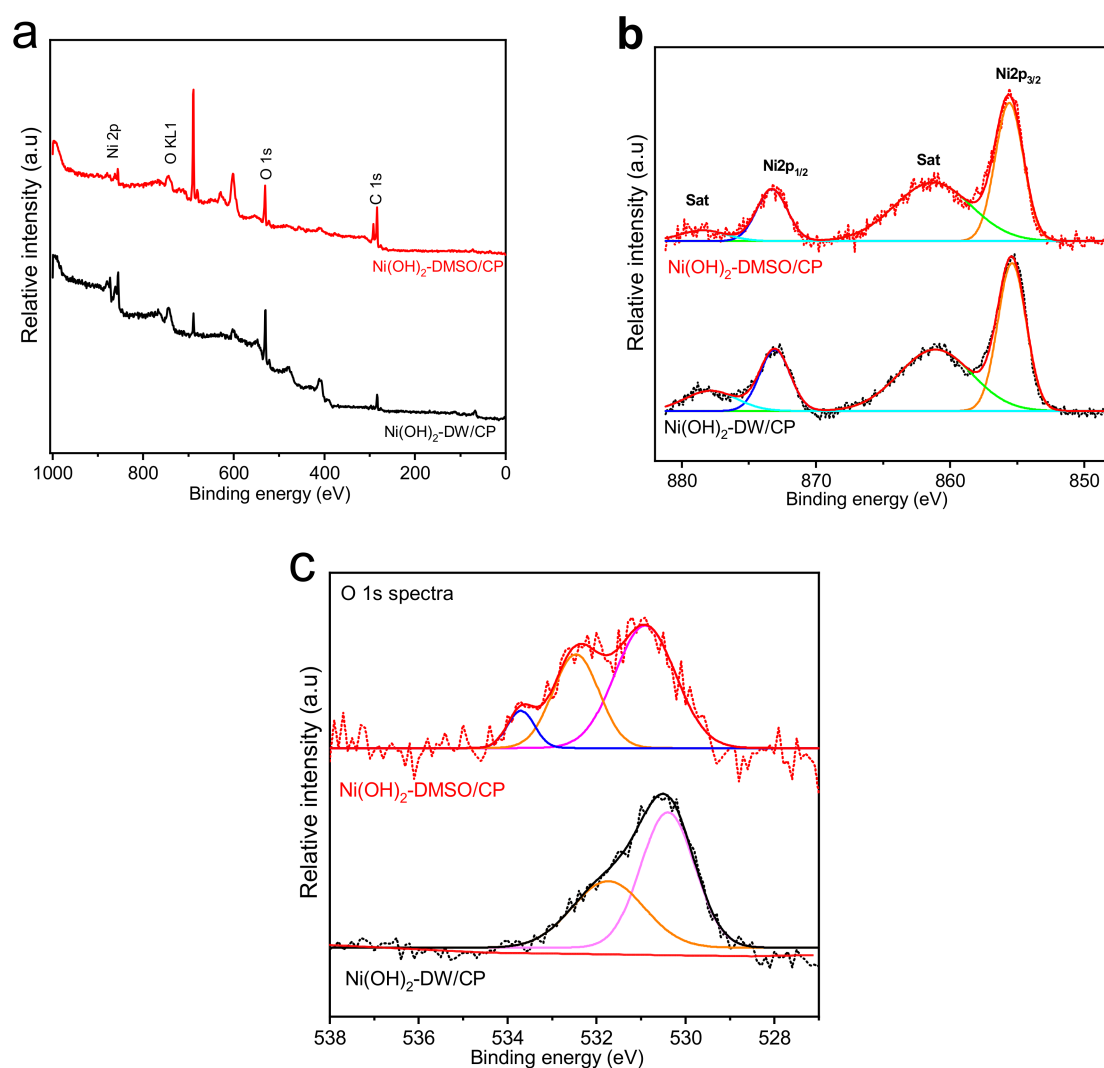


**Figure 3.** XPS spectra of (a) wide spectrum for Ni electrodeposits from all electrolytes, (b) Ni 2p spectra for Ni electrodeposits from both H<sub>2</sub>O and DMSO solutions, and (c) O 1s for the prepared catalyst from the DMSO electrolyte after electrodeposition and electrochemical measurements.

The solvent effect of the electrodeposited  $\text{Ni}(\text{OH})_2/\text{CP}$ -based materials was assessed via EDX examination. Notably, the EDAX-mapping examination disclosed the existence of Ni, C, and O components all through the  $\text{Ni}(\text{OH})_2\text{-DMSO/CP}$  catalyst (Supplementary Materials Figure S4). Noticeably, the EDAX-mapping revealed the identical arrangement of Ni and O over the CP substrate. It was also used to inspect the prepared electrodes surface chemical composition, as recorded in Table 1, and which pointed out that all deposits onto the CP made from various solvents contained Ni. In addition, C was found as a significant component of the carbon paper substrate. Notably, the EDX analysis confirmed that the trace amounts of nickel deposits were 0.70 more from DMSO than those from the aqueous solution (3.66%). The presence of F ions was attributed to the adhesive resin used in the preparation of the CP. The EDAX analysis displayed that the Ni/O ratio was almost 1:2, which perfectly matches the chemical composition of  $\text{Ni}(\text{OH})_2$  for  $\text{Ni}(\text{OH})_2\text{-DMSO}$  catalysts.

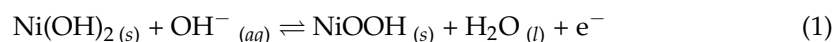
**Table 1.** Energy-dispersive X-ray spectroscopy (EDX) analysis of nickel catalyst deposited from various solutions: DW and DMSO.

Element, Atomic%	Carbon Paper (CP)	Ni, DW	Ni, DMSO
C K	82.56	54.09	84.36
O K	1.22	28.27	4.54
F K	16.22	13.97	10.15
Ni K	-	3.66	0.70
S K	-	-	0.09

The survey spectra XPS of the obtained catalyst from the DMSO solvent, as drawn in Figure 3a, pointed out the prominent characteristic peaks that the electrodeposits contained, with C, O, and Ni elements that were very close to the EDX analysis. In the case of the nickel electrodeposit from the water solution, the intensity of both  $\text{Ni } 2p_{3/2}$  and  $\text{Ni } 2p_{1/2}$  peaks was much stronger than that from the  $\text{Ni}(\text{OH})_2\text{-DMSO/CP}$  at the same binding energy, suggesting that the higher nickel content on the surface was from water media, as drawn in Figure 3b, which is consistent to that previously mentioned with EDX. Additionally, the amount of Ni in the fabricated  $\text{Ni}(\text{OH})_2/\text{CP}$  electrode materials prepared under DW and DMSO solution was assessed to be about 2 at.% (Supplementary Materials Table S1).

#### 2.4. Electrochemical Characterization of the $\text{Ni}(\text{OH})_2$ Catalyst

The electrochemical active surface area (ECSA) of the  $\text{Ni}(\text{OH})_2/\text{CP}$  electrocatalysts under the different employed solvents were initially examined by CV in alkaline media. Figure 4 displays the CVs at 50 mV/s of the electrochemical deposited  $\text{Ni}(\text{OH})_2$  over CP substrate in 1.0 M KOH in voltage varying from  $-0.2$  to  $0.6$  V vs. Ag/AgCl. Clearly, the electrocatalysts display a pair of redox peaks associated with about  $0.44$  V vs. Ag/AgCl, which are related to the characteristic of the  $\text{Ni(II)/Ni(III)}$  species [66,67], according to Equation (1).



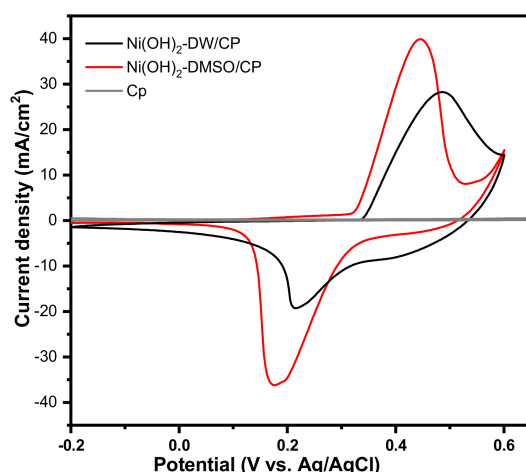


**Figure 4.** Cyclic voltammograms for  $\text{Ni(OH)}_2$  catalysts deposited from various electrolytes: DMSO and DW at scan rate 50 mV/s in 1.0 M KOH.

For the  $\text{Ni(OH)}_2$ -DMSO/CP electrodes, an oxidation peak of the distinctive passivation of Ni to  $(\text{Ni(OH)}_2/\text{NiOOH})$  took place, and whose peak moved towards greater current densities. Such a substantial upsurge in the current related to the oxidation peak resulted in a greater ECSA. Furthermore, the ECSA of the fabricated catalysts can be assessed according to the charge ( $Q$ ) area under the reduction peak. Via the equation ( $\text{ECSA} = Q/(mq)$ ), where  $Q$  is the charge required for the reduction of  $\text{NiOOH}$  to  $\text{Ni(OH)}_2$ ,  $m$  is the deposited quantity of the electrodes, and  $Q$  is the charge related to the creation of a monolayer of  $\text{Ni(OH)}_2$ , which equals  $257 \mu\text{C}/\text{cm}^2$  [22,48].

The ECSA values for  $\text{Ni(OH)}_2$ -DMSO/CP and  $\text{Ni(OH)}_2$ -DW/CP were found to be 2122.7 and  $634.3 \text{ m}^2/\text{g}$ , respectively, which suggests that the more active sites significantly resulted from the Ni film deposited from the DMSO solvent, which is in agreement with Figure 4. The higher surface area of  $\text{Ni(OH)}_2$ -DMSO/CP catalyst might be attributed to the low diffusion coefficient of Ni ions during the deposition process, due to its increased ability for creating polymer chains during the interactions between its sulfur and oxygen atoms, and the improvement of ion solvation–ion complex formation [68]. In addition, the roughness factors (RF), according to the equation:  $\text{RF} = \text{ECSA}/\text{geometric area}$ , can also be estimated at 8490.8 and 2537.2, for  $\text{Ni(OH)}_2$ -DMSO/CP and  $\text{Ni(OH)}_2$ -DW/CP, respectively. Evidently, the study reveals that  $\text{Ni(OH)}_2$ -DMSO/CP electrodes hold much superior ECSA and RF than  $\text{Ni(OH)}_2$ -DW/CP electrodes due to the generation of ultrathin nanoparticles.

Supplementary Materials Figure S5 represents the LSV at 50 mV/s for  $\text{Ni(OH)}_2$ -DMSO/CP, with different loadings in 1.0 M KOH. It clearly shows that as the catalyst loading increased, the OERs current also linearly increased. The urea onset potential moved nearly 50 mV to become more negative over the studied loading ranges, approving rapid kinetics for OERs.

The electrocatalytic features of the  $\text{Ni(OH)}_2$ -DMSO/CP electrocatalyst towards UORs in comparison with  $\text{Ni(OH)}_2$ -DW/CP benchmark catalysts were examined by CV, constant current/voltage, and EIS analysis under different operating conditions. The electrochemical UOR ability of the  $\text{Ni(OH)}_2$ -DMSO/CP was then evaluated in 1.0 M KOH in the presence (curve (ii)) and absence (curve (i)) of 0.33 M urea solution at 50 mV/s (Figure 5a). The CVs plot of the  $\text{Ni(OH)}_2$ -DMSO/CP electrode in the absence of urea revealed well-defined redox peaks ranging from 0.3 to 0.50 V vs. Ag/AgCl (Figure 5a), which are related to the coupled reactions of  $\text{Ni(OH)}_2$ . In the presence of 0.33 M urea, the prepared  $\text{Ni(OH)}_2$ -DMSO/CP catalysts displayed a substantial enhancement in the anodic current at the same onset potential that is consistent with the electrooxidation of the Ni(II) to Ni(III) peak. A urea oxidation peak at a more positive potential was observed at 0.35 V vs. Ag/AgCl, followed by the OER's higher potential. Moreover, the Ni(II)/Ni(III) redox center's reduction peak at 0.32 V vs. Ag/AgCl, during the reverse scan, comparatively decreased. This substantial



enrichment in the anodic current and the instantaneous vanishing of the cathodic peak in urea is coherent with the catalytic restoration of EC mechanisms [69]. A similar electrocatalytic mechanism is usually detected for the electrooxidation of smaller moieties, including methanol [70], ethanol [71], and glucose [72], as Ni-based electrodes are engaged under the basic medium.

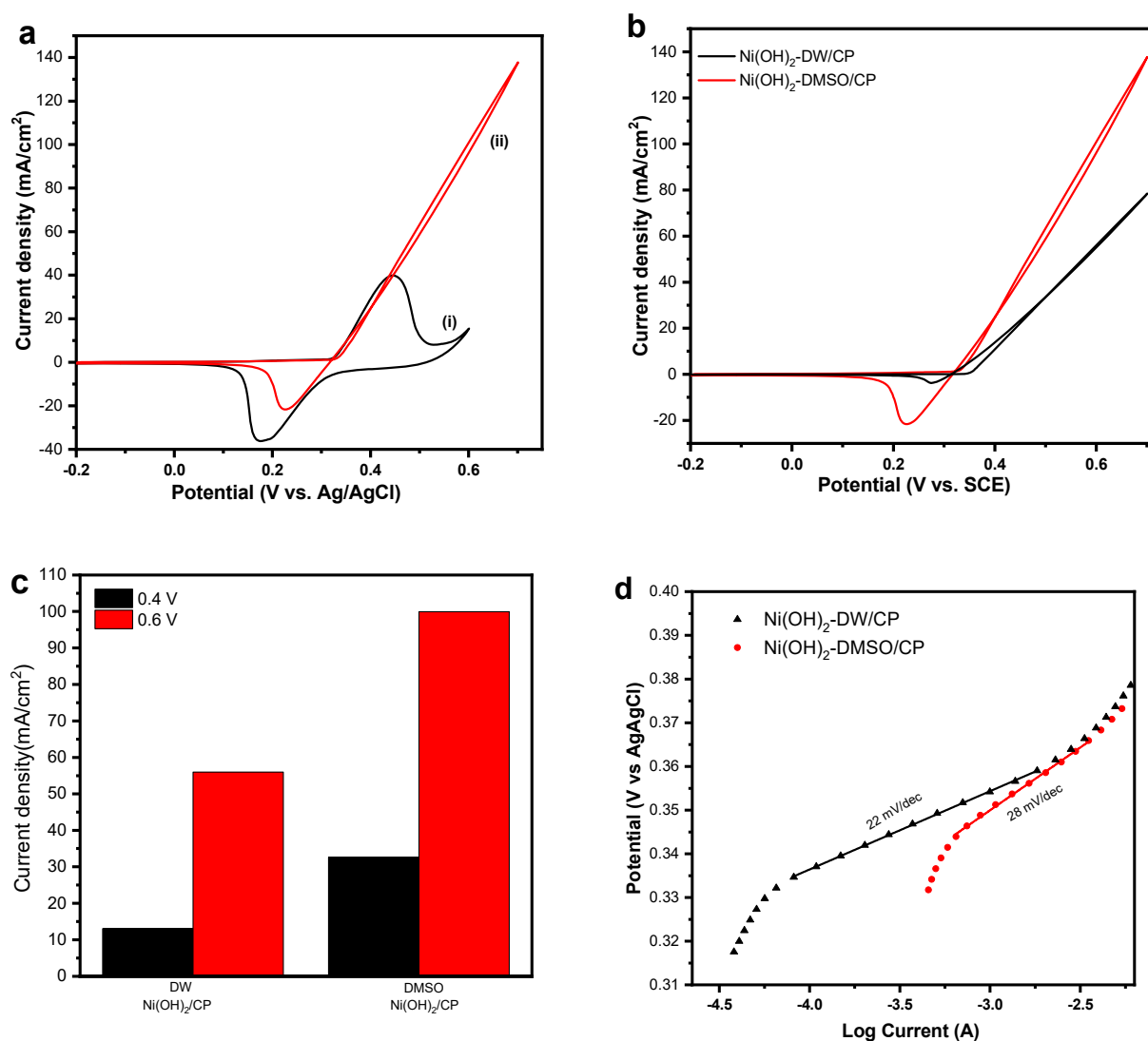


**Figure 5.** (a) Cyclic voltammetric analysis at 50 mV/s for the Ni(OH)<sub>2</sub>-DMSO/CP electrode in the absence (i) and in the presence of 0.33 M urea in 1.0 M KOH (ii), (b) CVs for Ni(OH)<sub>2</sub>/CP catalysts deposited from deionized water (DW), and DMSO in 0.33 M urea/KOH, (c) The current density of the Ni(OH)<sub>2</sub>/CP electrodes prepared with different solvents at the potential of 0.4 V and 0.6 V vs. Ag/AgCl. (d) Tafel slope of the polarization curves in (Figure 5b).

As shown in Figure 5b, the electrochemical UORs featuring of all the different solvent samples were then measured in 1.0 M KOH, with 0.33 M urea solution at 50 mV/s. A superior anodic current response was recorded for all the samples after 0.30 V, signifying the more remarkable ability for electrochemical UORs. No nickel oxidation peak was witnessed in the positive scan direction, signifying the total occupation of adsorbed urea on the active sites. Furthermore, the electrooxidation of Ni(OH)<sub>2</sub> to NiOOH must occur at the higher potentials associated with the UOR process, owing to the contribution of NiOOH (vide infra). Furthermore, by comparing the current density of Ni(OH)<sub>2</sub>-DMSO/CP and Ni(OH)<sub>2</sub>-DW/CP samples at 0.5 V, the Ni(OH)<sub>2</sub>-DMSO/CP had about a two times superior current density to that of Ni(OH)<sub>2</sub>-DW/CP, demonstrating the importance of surface

area enhancement. Moreover, the UOR potentials at  $10 \text{ mA cm}^{-2}$  for  $\text{Ni(OH)}_2\text{-DMSO/CP}$  and  $\text{Ni(OH)}_2\text{-DW/CP}$  were 0.35 V and 0.382 V, respectively, indicating a 32 mV decrease in the case of the DMSO solution. Specifically, the peak current density was 0.4 and 0.6 V vs. Ag/AgCl, as displayed in Figure 5c, for a perfect comparison. The  $\text{Ni(OH)}_2\text{-DMSO/CP}$  electrodes' maximum current density could reach ca.  $99.9 \text{ mA cm}^{-2}$  at 0.6 V vs. Ag/AgCl, which was greater than the  $\text{Ni(OH)}_2\text{-DW/CP}$  ( $55.9 \text{ mA cm}^{-2}$ ). Here it was clearly evidenced that the  $\text{Ni(OH)}_2\text{-DMSO/CP}$  electrodes had the greater electrocatalytic ability for electrochemical UORs. These electrochemical activity differences might come from the changes in the surface area, as shown by the different reversibilities for the Ni(II)/Ni(III) redox position and the ECSA, as well as the catalytic kinetics (vide infra). Moreover, the Tafel analysis (Figure 5d) provides Tafel slopes of 22 and  $28 \text{ mV dec}^{-1}$  for  $\text{Ni(OH)}_2\text{-DW/CP}$  and  $\text{Ni(OH)}_2\text{-DMSO/CP}$ , correspondingly. Notably, thus, the better catalytic features for UORs were obtained, owing to the enhanced charge-transfer rate and the rapid kinetics through the electrochemical UOR process.

To inspect the influence of KOH concentration over electrochemical UORs, Figure 6a shows the CV at 50 mV/s of  $\text{Ni(OH)}_2\text{-DMSO/CP}$  catalysts in 0.33 M urea. The bare-CP catalysts reveal no significant current for the electrochemical UORs, specifying that the bare electrode has no apparent electrocatalytic features towards UORs. Notably, the UOR current ( $I_p$ ) during the forward scan was around  $60 \text{ mA cm}^{-2}$  at 0.5 V, superior to 1.0 M KOH. In addition, the onset potential of UORs was considerably moved to a lesser potential (about 105 mV), indicating that the electrochemical UORs become thermodynamically more favorable under higher alkaline conditions. As described via Botte et al. [69], when the KOH increases, a negative shift in the oxidation potential can be observed, while an upsurge in electrocatalytic UORs current with a decrease in the reduction peak of NiOOH is witnessed with the presence of urea (Figure 6b). This result can be attributed to the more substantial influence of OH ions on creating NiOOH species that successively catalyze the UORs. More importantly, this phenomenon was demonstrated in recent reports [59,63,64], associated with more depletion of NiOOH through UORs in a higher concentrated solution. This  $\text{EC}^-$  mechanism was evidenced via in-situ Raman spectroscopy, and the obtained product of UORs was  $\text{CO}_2$  and  $\text{N}_2$  gas in a basic environment [69].

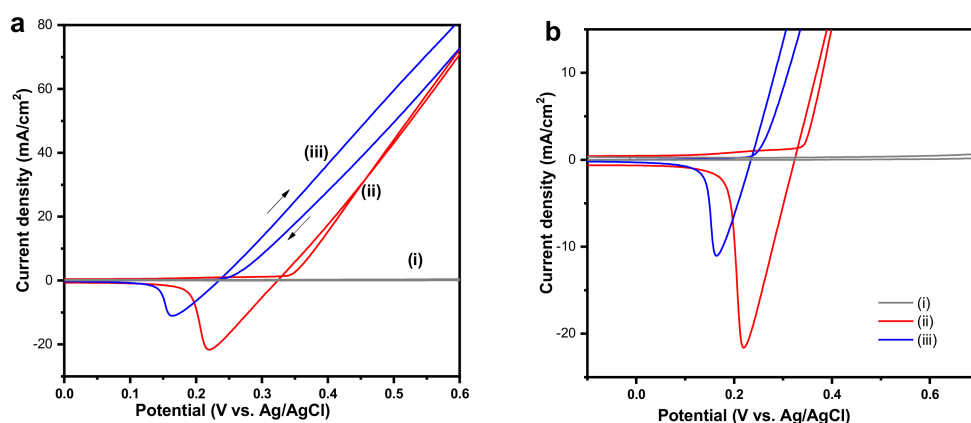


**Figure 6.** (a) CVs at 50 mV/s for bare-CP (i), and  $\text{Ni(OH)}_2\text{-DMSO/CP}$  electrodes (ii) prepared under DMSO solution in 0.33 M urea and 1.0 M KOH;  $\text{Ni(OH)}_2\text{-DMSO/CP}$  electrodes in 0.33 M urea and 5.0 M KOH (iii), (b) displays an enlarged view.

The urea concentrations in electrochemical reactions significantly influence the UORs at Ni-based electrodes, as described by Botte et al. [69]. In this regard, the urea concentration in 1.0 M KOH was examined. Shown in Figure 7a,b, is the anodic peak of the UORs at the  $\text{Ni(OH)}_2\text{-DMSO/CP}$  catalysts; the forward scan upsurged linearly to 0.33 M urea and then decreased at higher concentrations. Notably, the electrooxidation of current upsurged linearly, ascribed to the electrochemical UORs under diffusion-control when the

urea concentrations were below 0.33 M [69]. In addition, Figure 7c reveals the influence of increasing urea concentration on the vanishing of the Ni(III)/Ni(II) reduction peak at  $-0.25$  V vs. Ag/AgCl. Evidently, Figure 7c shows higher urea concentrations, resulting in a gradual decline in the Ni(III)/Ni(II) cathodic reduction peak current. Remarkably, the electrocatalytic UORs at the Ni(OH)<sub>2</sub>-DMSO/CP electrodes under basic media follow the EC mechanisms, and increase the urea concentration, generating more NiOOH; a decline in reduction peak currents are observed [69].

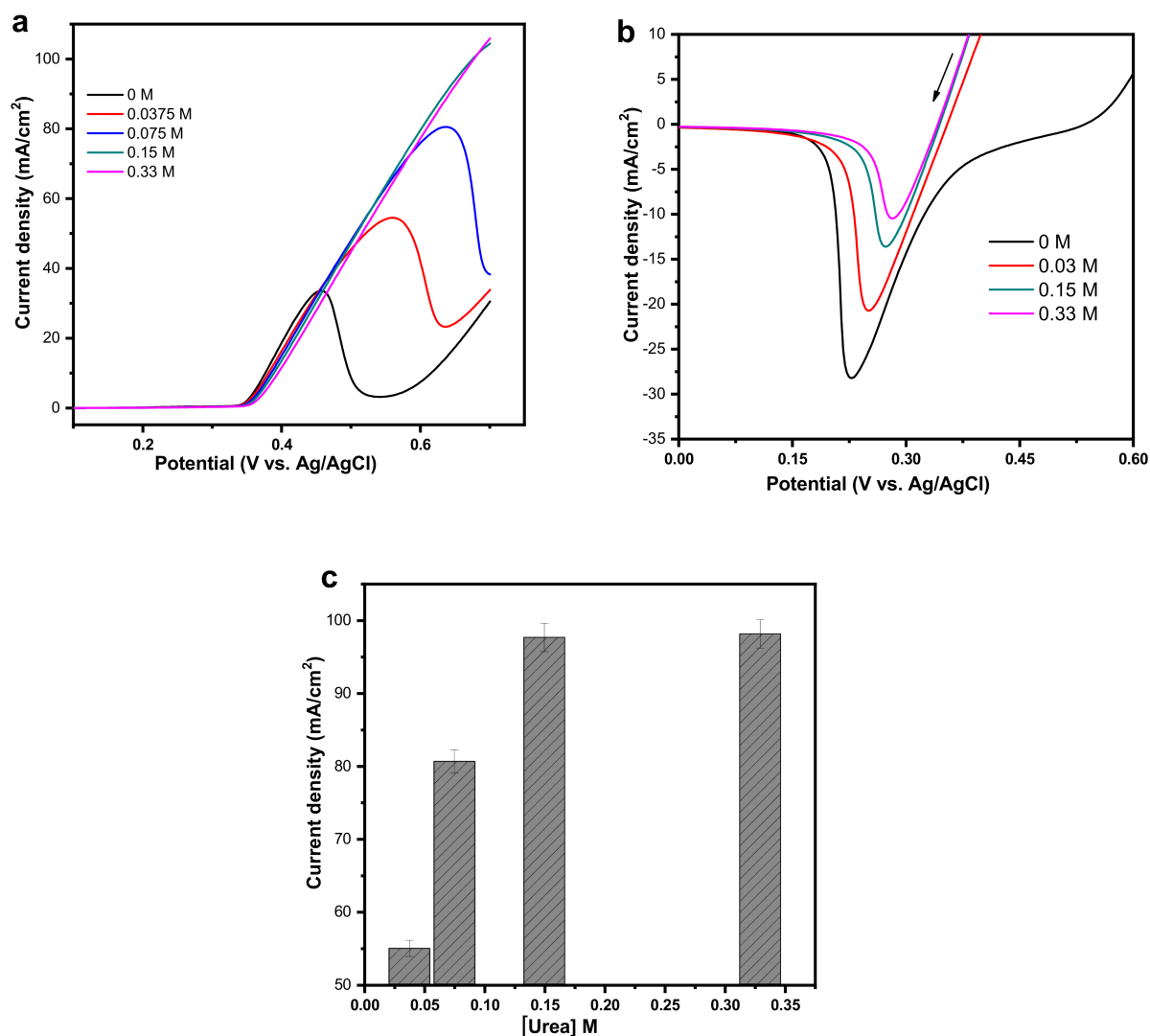


**Figure 7.** Cyclic voltammetry at 50 mV/s for Ni(OH)<sub>2</sub>-DMSO/CP catalyst in 1.0 M KOH and at various urea concentrations: (a) forward scan/(b) backward scan, and (c) displays the plot for the different urea concentrations against the anodic oxidation peak.

The electrochemical durability test of the Ni(OH)<sub>2</sub>-DMSO/CP catalysts for the UOR in 0.33 mol/L urea was applied by multicycle voltammetry and chronoamperometry at 0.5 V vs. Ag/AgCl for 3500 s. The potential multicycle voltammetry in Figure 8a shows the Ni(OH)<sub>2</sub>-DMSO/CP catalysts in 1.0 M KOH and 0.33 M urea. The result of the potential multicycles exhibited that the electrochemical UORs current at Ni(OH)<sub>2</sub>-DMSO/CP electrode was nearly steady, and the analogous CV was replicated without any deleterious features up to 50 cycles. However, after 50 cycles, the electrochemical UORs current was marginally decreased by approximately 10%, apparently owing to the electrocatalyst's physical detachment from the surface. Figure 8b shows that the



chronoamperometric measurement of the  $\text{Ni(OH)}_2\text{-DMSO/CP}$  electrode prepared in the DMSO solution was superior to that of other electrode materials, demonstrating highly active and durable features for UORs in basic media. The current fluctuation during the electrocatalytic test was mainly due to delivering gaseous products that adsorbed on the electrode surface [73]. For the electrocatalytic durability, activity decay was initiated by carbon monoxide's adsorption on both nickel-based catalysts during the electrochemical process [23,74]. The chronopotentiometry responses of  $\text{Ni(OH)}_2\text{-DMSO/CP}$  catalysts were evaluated for 10 h at  $25 \text{ mA/cm}^2$  constant current in 0.33 M urea and 1.0 M KOH (Figure 8c). The long-term durability analysis of the  $\text{Ni(OH)}_2\text{-DMSO/CP}$  catalysts revealed that the current density was very stable, with no apparent loss during the UORs. This indicates that the  $\text{Ni(OH)}_2$  based electrodes prepared with organic DMSO solution have exceptional durability and good electrocatalytic UOR features.

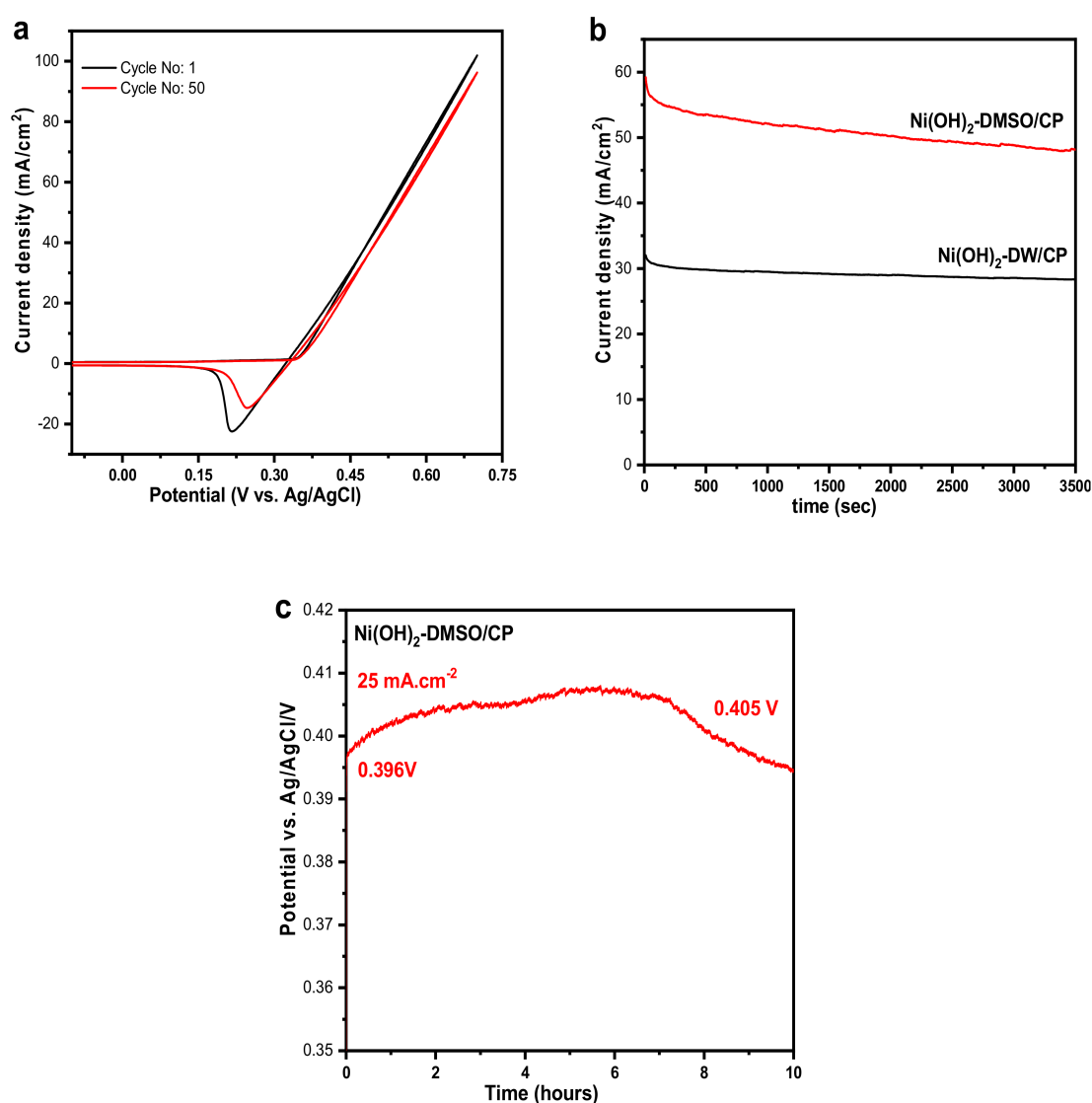


**Figure 8.** (a) Cycle voltammetric analysis (1st and 50th cycles) of the  $\text{Ni(OH)}_2\text{-DMSO/CP}$  electrode at a sweep rate of 50 mV/s in 1.0 M KOH/0.33 M urea, (b) Chronoamperometry curves during the electrooxidation of 0.33 M urea and 1.0 M KOH at different  $\text{Ni(OH)}_2\text{/CP}$  electrodes, prepared under different solvents at 0.5 V vs. Ag/AgCl, (c) Chronopotentiometric response of the  $\text{Ni(OH)}_2\text{-DMSO/CP}$  electrode at a  $25 \text{ mA/cm}^2$  constant current in 0.33 M urea and 1.0 M KOH.

Comparing the electrocatalytic features of our  $\text{Ni(OH)}_2\text{-DMSO/CP}$  catalysts with earlier published works relating to Ni containing electrocatalytic materials, Table 2, pro-

vides an assessment of the electrocatalytic specific activity and analysis circumstances of the  $\text{Ni}(\text{OH})_2$ -DMSO/CP, and other associated nickel-containing catalysts investigated in the literature [23,24,28,34,74–76]. Evidently, our  $\text{Ni}(\text{OH})_2$ -DMSO/CP electrodes are significantly more better than the reported catalysts, confirming that this catalyst provides more reactive sites. These results evidenced that the  $\text{Ni}(\text{OH})_2$ -DMSO strongly enhanced the electrochemical performance of electrochemical UORs.

**Table 2.** Comparison of the electrocatalytic UOR of various nickel-containing catalysts in 0.33 M urea/1.0 M KOH according to CV curves.

Anodic Materials	Specific Activity/Mass Activity $\text{mA}/\text{cm}^2$	Tafel Plot/ $\text{mVdec}^{-1}$	Stability	Onset Potential, V	References
$(\text{Ni}-\text{WO}_2)/\text{C}/\text{NF}$	$300 \text{ mA}/\text{cm}^2/-$	33	80 h	1.30 vs. RHE	[24]
$\text{Ni}-\text{NiO}-\text{Mo}_{0.84}\text{Ni}_{0.16}/\text{NF}$	$400 \text{ mA}/\text{cm}^2/-$	35.78	60 h	1.33 vs. RHE	[75]
$\text{Ni}/\text{C}-\text{V}_2\text{O}_3/\text{NF}$	$1200 \text{ mA}/\text{cm}^2/-$	41.22	50 h	1.32 vs. RHE	[76]
$\text{NiO}/\text{Gt}$ electrocatalyst	$\sim 30 \text{ mA}/\text{cm}^2/-$	116.08	0.5 h	0.345 V vs. Ag/AgCl	[34]
Ni-Deposited Sn Dendrites	$44 \text{ mA}/\text{cm}^2/-$	-	$\sim 1.0$ h	0.34 V vs. Ag/AgCl	[77]
$\text{Ni}(\text{OH})_2$ nanomesh	$-/800 \text{ mA}/\text{mg}$	80	1.5 h	1.38 V vs. RHE	[28]
$\text{La}_{0.5}\text{Sr}_{1.5}\text{NiO}_4 + \delta$ (LSN25)	$-/1200 \text{ mA}/\text{mg}$	-	1.0 h	0.44 V vs. Hg/HgO	[53]
$\text{Ni}(\text{OH})_2$ nanoflakes	$-/1295 \text{ mA}/\text{mg}$	-	1.0 h	0.38 V vs. SCE	[78]
$\text{Ni}(\text{OH})_2$ -DMSO	$100 \text{ mA}/\text{cm}^2/1000 \text{ mA}/\text{mg}$	28	5.0 h	0.5 V vs. Ag/AgCl	This work
$\text{Ni}(\text{OH})_2$ -H <sub>2</sub> O	$56 \text{ mA}/\text{cm}^2$	22		0.5 V vs. Ag/AgCl	This work

The  $\text{Ni}(\text{OH})_2$ /CP based electrode's excellent performance is evidenced by the electrochemical impedance analysis (Figure 9a). As seen in Figure 9a, the semicircle diameter of all the investigated electrodes followed the order  $\text{Ni}(\text{OH})_2$ -DMSO/CP <  $\text{Ni}(\text{OH})_2$ -DW/CP. Furthermore, the EIS spectrum was best-fitted by a characteristic equivalent circuit (Figure 9a). The equivalent circuit comprises a parallel combination of ( $\text{Rct}_1$ ,  $\text{CPE}_1$ ), and ( $\text{Rct}_2$ ,  $\text{CPE}_2$ ) elements in series with  $\text{R}_s$ . It is clearly evidenced that the  $\text{Ni}(\text{OH})_2$ -DMSO/CP electrodes prepared in DMSO solution offer a lower arc radius on the EIS Nyquist plot, indicating that it has a smaller  $\text{Rct}_2$  ( $1.16 \Omega$ ) and better electrochemical performance compared with a value of  $6.10 \Omega$  for  $\text{Ni}(\text{OH})_2$ -DW/CP catalysts (Figure 9a and Supplementary Materials Table S2). Moreover, Figure 9b reveals the Nyquist spectra for  $\text{Ni}(\text{OH})_2$ -DMSO/CP catalyst at various voltages from 0.40–0.60 V in 0.33 M urea/KOH, in which the semicircle diameter and  $\text{Rct}_2$  values were significantly decreased as the voltage shifted from 0.40 to 0.60 V vs. Ag/AgCl, which indicates that the urea electrooxidation process at the  $\text{Ni}(\text{OH})_2$ -DMSO/CP electrode is considerably improved at higher potentials, consistent with the cyclic voltammetry results above.

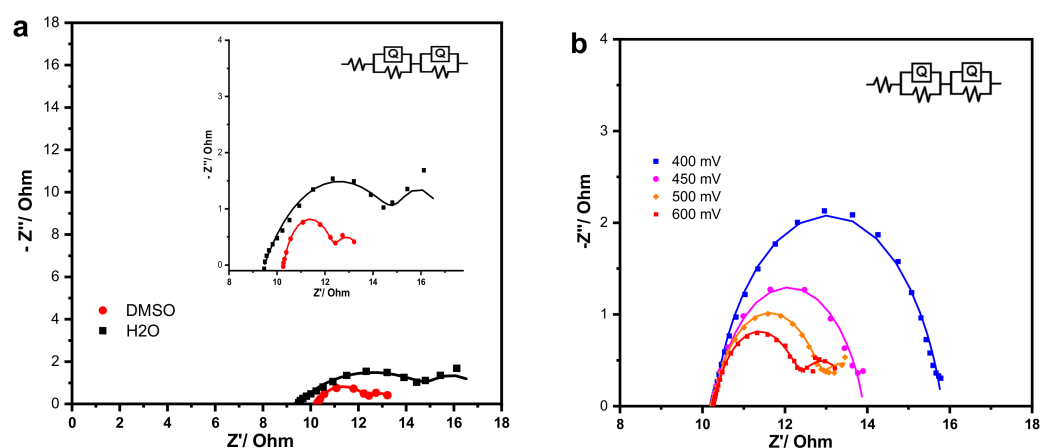


**Figure 9.** (a) Nyquist plots of the  $\text{Ni(OH)}_2/\text{CP}$  electrodes, the inset plot displays the equivalent circuit model; (b) and its corresponding Nyquist plot obtained for the  $\text{Ni(OH)}_2\text{-DMSO/CP}$  electrode logged at various voltages in 1.0 M KOH containing 0.33 M urea.

### 3. Experimental

#### 3.1. Materials

Anhydrous nickel chloride ( $\text{NiCl}_2$ , 99.0%) was acquired from Alfa Aesar (Ward Hill, MA, USA). Urea was acquired from AVONCHEM Corp (Macclesfield, Cheshire, UK). Dimethylsulphoxide (DMSO, 99.0%) was purchased from LOBA Chemie (Mumbai, India). CP substrate (SIGRACETR, grade GDL-24BC, SGL) was used as a working electrode. Pure potassium hydroxide pellets (KOH, 85.0%) were obtained from the AnalaR group (Berwyn, PA, USA).

#### 3.2. Synthesis of $\text{Ni(OH)}_2/\text{CP}$ Catalysts

The  $\text{Ni(OH)}_2/\text{CP}$  electrodes were obtained by electrodeposition from organic and aqueous complexes directly on the CP's surface. Before the electrodeposition process, a commercial carbon paper ( $^{\text{®}}$ SIGRACET, GDL = 248 C;  $0.5 \times 0.5 \text{ cm}^2$ ) was pre-treated in a hot concentrated  $\text{HNO}_3$ , at  $70^\circ\text{C}$  for 60 s, then rinsed with  $\text{H}_2\text{O}$  and allowed to dry overnight. The electrodeposition process was carried out using a  $\mu\text{-AutolabIII/FRA2}$  potentiostat/galvanostat via a three-electrode cell. The cell comprised Pt wire and saturated Ag/AgCl as counter and reference electrodes, respectively. In addition, a working electrode was composed of treated CP. The deposition solution contained 0.02 M anhydrous  $\text{NiCl}_2$  dissolved into 100 mL of DMSO solvents, or DW, and left sealed in a glass flask for 24 h before use. A controlled deposition program was applied with a deposition charge of  $320 \mu\text{C}/\text{cm}^2$  with 10 repetitions of 10 s at  $-2.0 \text{ V}$ , then subjected to the oxidative potential cycling ( $-0.2 \text{ V}$  to  $+0.6 \text{ V}$  at  $50 \text{ mV/s}$ ) in an alkaline solution of 1.0 M KOH for 10 cycles [79,80].

#### 3.3. Materials Characterization

Powder X-ray diffraction (XRD) data were obtained via a MiniFlex-600 (Rigaku) with Cu K $\alpha$  irradiation (40 kV, 15 mA). The field-emission scanning electron microscope (FE-SEM) images were logged on a JSM-7610F functioned at 15 kV, and armed with an energy-dispersive X-ray spectroscopy (EDX) analyzer. To examine the surface elements composition with their oxidation states, X-ray photoemission spectroscopy (XPS) analysis was conducted by employing an Escalab 250 spectrometer. A high-resolution transmission electron microscope (HR-TEM) study was recorded with a JEOL 2100F (Japan), functioned at 200 kV, to detect the internal structure.

Electrochemical analysis was performed using a  $\mu\text{-AutolabIII/FRA2}$  potentiostat/galvanostat, commanded by NOVA1.11 software, directly connected into a classical three-electrode electrochemical cell. The cell comprised deposited catalysts on a CP substrate's



conductivity side as a working electrode ( $0.25\text{ cm}^2$ ), and was employed in a three-electrode setup during the measurements. The electrochemical measurements of the fabricated electrodes were first examined in a basic solution of  $1.0\text{ M KOH}$ , then this solution containing  $0.33\text{ M urea}$  was examined by cyclic voltammetry experiments (CVs), chronoamperometric techniques (CA), and electrochemical impedance spectroscopy (EIS). The latter measurements were conducted at various potentials through frequencies from  $0.05\text{ Hz}$  to  $100\text{ kHz}$ . The  $\text{Ni(OH)}_2$  electrodes were obtained by a facile electrodeposition method, without any additives, and at optimal electrodeposition of  $320\text{ }\mu\text{C}/\text{cm}^2$  at  $-2.0\text{ V}$  vs.  $\text{Ag}/\text{AgCl}$  from DMSO, and with  $\text{H}_2\text{O}$  solvent to CP substrate denoted as  $\text{Ni(OH)}_2\text{-DMSO/CP}$  and  $\text{Ni(OH)}_2\text{-DW/CP}$ , respectively.

#### 4. Conclusions

In summary, a facile strategy has been successfully demonstrated for synthesizing electrocatalysts of  $\text{Ni(OH)}_2$  nanostructure onto carbon paper for urea electrolysis via a cost-effective electrodeposition method from organic electrolyte of DMSO, and also an aqueous solution ( $\text{H}_2\text{O}$ ). The physicochemical characterizations confirmed the creation of a  $\text{Ni(OH)}_2$  nanoparticles catalyst, and the obtained  $\text{Ni(OH)}_2$  catalyst deposited from the DMSO solvent exhibited excellent stability and electrocatalytic activity toward electrochemical urea oxidation, due to its high ESA value  $2122.7\text{ m}^2/\text{g}$ . The electrochemical assessments revealed that the  $\text{Ni(OH)}_2$  deposited in the DMSO medium effectually improved the electrochemical UORs at a lower potential with greater activity over the reported  $\text{Ni(OH)}_2$  containing catalysts. The results would provide a simple and inexpensive way to activate commercial carbon paper with  $\text{Ni(OH)}_2$ , an abundant earth transition metal hydroxide, for urea electrolysis, and show a broad range of direct urea applications for fuel cells and clean energy generation.

**Supplementary Materials:** The following are available online at <https://www.mdpi.com/2073-4344/11/1/102/s1>, Figure S1: HRTEM analysis; Figure S2: EDAX mapping analysis; Figure S3: XRD analysis of electrodeposited  $\text{Ni(OH)}_2$  electrodes; Figure S4: SEM and the EDX profile of C, Ni, and O elements of  $\text{Ni(OH)}_2\text{-DMSO/CP}$  (C) electrodes prepared with DMSO medium; Figure S5: Cyclic voltammograms for  $\text{Ni(OH)}_2$  catalysts deposited from different deposition charge from DMSO and at scan rate  $50\text{ mVs}^{-1}$  in the presence of  $1.0\text{ M KOH}$ ; Table S1: XPS analysis of  $\text{Ni(OH)}_2\text{/CP}$  electrodes obtained from various solutions: DMSO and  $\text{H}_2\text{O}$ ; Table S2: EIS parameters involving  $R_s$ ,  $R_{ct1}$ ,  $R_{ct2}$ ,  $\text{CPE}_1$  and  $\text{CPE}_2$  elements for  $\text{Ni(OH)}_2$  catalysts deposited from DMSO and  $\text{H}_2\text{O}$  solutions at various potentials in  $0.33\text{ M urea/KOH}$ .

**Author Contributions:** Conceptualization: M.N.S., A.M.A.-M., P.A.; Formal Analysis: S.A.A.; Funding Acquisition: A.M.A.-M.; Investigation: S.A.A., M.S.A.; Methodology: N.H.A., N.K.A.; Supervision: A.M.A.-M., M.A.G., P.A.; Visualization: P.A., M.A.G.; Writing—Original Draft Preparation: S.A.A., P.A.; Writing—Review and Editing: P.A., M.A.G. All authors have read and agreed to the published version of the manuscript.

**Funding:** The authors are grateful to the Deanship of Scientific Research, King Saud University, for funding through the Vice Deanship of Scientific Research Chairs. Saba A. Aladeemy thanks the student support program provided by K.A.CARE. Mabrook S. Amer thanks the postdoc program supported by K.A.CARE for King Saud University.

**Institutional Review Board Statement:** Not applicable.

**Informed Consent Statement:** Not applicable.

**Data Availability Statement:** Data is contained within the article or supplementary material.

**Acknowledgments:** The authors are grateful to the Deanship of Scientific Research, King Saud University, for funding through the Vice Deanship of Scientific Research Chairs. Saba A. Aladeemy thanks the student support program provided by K.A.CARE. Mabrook S. Amer thanks the postdoc program supported by K.A.CARE for King Saud University.

**Conflicts of Interest:** The authors declare no conflict of interest.

## References

- Kim, J.; Monllor-Satoca, D.; Choi, W. Simultaneous production of hydrogen with the degradation of organic pollutants using TiO<sub>2</sub> photocatalyst modified with dual surface components. *Energy Environ. Sci.* **2012**, *5*, 7647–7656. [\[CrossRef\]](#)
- Rollinson, A.N.; Jones, J.; Dupont, V.; Twigg, M.V. Urea as a hydrogen carrier: A perspective on its potential for safe, sustainable and long-term energy supply. *Energy Environ. Sci.* **2011**, *4*, 1216–1224. [\[CrossRef\]](#)
- Ji, R.; Chan, D.; Jow, J.; Wu, M. Formation of open-ended nickel hydroxide nanotubes on three-dimensional nickel framework for enhanced urea electrolysis. *Electrochem. Commun.* **2013**, *29*, 21–24. [\[CrossRef\]](#)
- Boggs, B.K.; King, R.L.; Botte, G.G. Urea electrolysis: direct hydrogen production from urine. *Chem. Commun.* **2009**, 4859–4861. [\[CrossRef\]](#) [\[PubMed\]](#)
- Yan, W.; Wang, D.; Botte, G.G. Nickel and cobalt bimetallic hydroxide catalysts for urea electro-oxidation. *Electrochim. Acta* **2012**, *61*, 25–30. [\[CrossRef\]](#)
- Terblanche, A.P.S. Health hazards of nitrate in drinking water. *Water S.A.* **1991**, *17*, 77–82.
- Simka, W.; Piotrowski, J.; Robak, A.; Nawrat, G. Electrochemical treatment of aqueous solutions containing urea. *J. Appl. Electrochem.* **2009**, *39*, 1137–1143. [\[CrossRef\]](#)
- Patzer, J.F., II; Wolfson, S.K., Jr.; Yao, S.J. Platinized-titanium electrodes for urea oxidation Part II. Concentric spiral coil geometry. *J. Mol. Catal.* **1991**, *70*, 231–242. [\[CrossRef\]](#)
- Wright, J.C.; Michaels, A.S.; Appleby, A.J. Electrooxidation of urea at the ruthenium titanium oxide electrode. *AIChE J.* **1986**, *32*, 1450–1458. [\[CrossRef\]](#)
- Lan, R.; Tao, S.; Irvine, J.T.S. A direct urea fuel cell—power from fertiliser and waste. *Energy Environ. Sci.* **2010**, *3*, 438. [\[CrossRef\]](#)
- Barakat, N.A.M.; El-Newehy, M.H.; Yasin, A.S.; Ghouri, Z.K.; Al Deyab, S.S. Ni&Mn nanoparticles-decorated carbon nanofibers as effective electrocatalyst for urea oxidation. *Appl. Catal. A* **2016**, *510*, 180–188.
- Tong, Y.; Chen, P.; Zhang, M.; Zhou, T.; Zhang, L.; Chu, W.; Wu, C.; Xie, Y. Oxygen vacancies confined in nickel molybdenum oxide porous nanosheets for promoted electrocatalytic urea oxidation. *ACS Catal.* **2018**, *8*, 1–7. [\[CrossRef\]](#)
- Basumatary, P.; Konwar, D.; Yoon, Y.S. A novel NiCu/ZnO@MWCNT anode employed in urea fuel cell to attain superior performances. *Electrochim. Acta* **2018**, *261*, 78–85. [\[CrossRef\]](#)
- Gromyko, V.A.; Tsygankova, T.B.; Gaidadymov, V.B.; Vasil'ev, Y.B.; Bagotskii, V.S. Elektrooxidation von harnstoff an einer glatten platinelektrode 2. Mitt. *Elektrokhimiya* **1974**, *10*, 57.
- Horanyi, G.; Inzelt, G.; Rizmayer, E.M. Radiotracer study of the adsorption of urea on platinized platinum electrodes in the presence of different ions and organic compounds. *J. Electroanal. Chem. Interfacial Electrochem.* **1979**, *98*, 105. [\[CrossRef\]](#)
- Ling, T.R.; Lien, K.T.; Jow, J.J.; Lin, T.Y. Mesoporous Nickel Electrode for the Detection of Alcohol. *Electroanalysis* **2009**, *21*, 2213–2219. [\[CrossRef\]](#)
- Arunachalam, P.; Nagarani, S.; Prasad, S.; AlSalhi, M.S.; Al-Mayouf, A.M.; Moydeen, M.; Ganapathy, S. Facile coprecipitation synthesis of nickel doped copper oxide nanocomposite as electrocatalyst for methanol electrooxidation in alkaline solution. *Mater. Res. Express* **2018**, *5*, 015512. [\[CrossRef\]](#)
- Arunachalam, P.; Shaddad, M.N.; Alamoudi, A.S.; Ghanem, M.A.; Al-Mayouf, A.M. Microwave-assisted synthesis of Co<sub>3</sub>(PO<sub>4</sub>)<sub>2</sub> nanospheres for electrocatalytic oxidation of methanol in alkaline media. *Catalysts* **2017**, *7*, 119. [\[CrossRef\]](#)
- Al-Sharif, M.S.; Arunachalam, P.; Abiti, T.; Amer, M.S.; Al-Shalwi, M.; Ghanem, M.A. Mesoporous cobalt phosphate electrocatalyst prepared using liquid crystal template for methanol oxidation reaction in alkaline solution. *Arabian J. Chem.* **2020**, *13*, 2873–2882. [\[CrossRef\]](#)
- El-Shafei, A.A.J. Electrocatalytic oxidation of methanol at a nickel hydroxide/glassy carbon modified electrode in alkaline medium. *Electroanal. Chem.* **1999**, *471*, 89–95. [\[CrossRef\]](#)
- Yan, W.; Wang, D.; Botte, G.G. Template-assisted synthesis of Ni–Co bimetallic nanowires for urea electrocatalytic oxidation. *J. Appl. Electrochem.* **2015**, *45*, 1217–1222. [\[CrossRef\]](#)
- Yan, W.; Wang, D.; Diaz, L.A.; Botte, G.G. Nickel nanowires as effective catalysts for urea electro-oxidation. *Electrochimica Acta* **2014**, *134*, 266–271. [\[CrossRef\]](#)
- Chen, J.; Ci, S.; Wang, G.; Senthikumar, N.; Zhang, M.; Xu, Q.; Wen, Z. Ni(OH)<sub>2</sub> Nanosheet Electrocatalyst toward alkaline urea electrolysis for energy-saving acidic hydrogen production. *ChemElectroChem* **2019**, *6*, 5313–5320. [\[CrossRef\]](#)
- Abdel Hameed, R.M.; Medany, S.S. Influence of support material on the electrocatalytic activity of nickel oxide nanoparticles for urea electro-oxidation reaction. *J. Colloid Interface Sci.* **2018**, *513*, 536–548. [\[CrossRef\]](#) [\[PubMed\]](#)
- Chen, P.H. Platinum-based nanostructured materials: synthesis, properties, and applications. *Hindle Chem. Rev.* **2010**, *110*, 3767–3804. [\[CrossRef\]](#) [\[PubMed\]](#)
- Sun, X.; Ding, R. Recent progress with electrocatalysts for urea electrolysis in alkaline media for energy-saving hydrogen production. *Catal. Sci. Technol.* **2020**, *10*, 1567–1581. [\[CrossRef\]](#)
- Wang, G.; Wen, Z. Self-supported bimetallic Ni–Co compound electrodes for urea-and neutralization energy-assisted electrolytic hydrogen production. *Nanoscale* **2018**, *10*, 21087–21095. [\[CrossRef\]](#)
- Ding, Y.; Li, Y.; Xue, Y.; Miao, B.; Li, S.; Jiang, Y.; Liu, X.; Chen, Y. Atomically thick Ni(OH)<sub>2</sub> nanomeshes for urea electrooxidation. *Nanoscale* **2019**, *11*, 1058–1064. [\[CrossRef\]](#)
- Wei, S.; Wang, X.; Wang, J.; Sun, X.; Cui, L.; Yang, W.; Zheng, Y.; Liu, J. CoS<sub>2</sub> nanoneedle array on Ti mesh: a stable and efficient bifunctional electrocatalyst for urea-assisted electrolytic hydrogen production. *Electrochim. Acta* **2017**, *246*, 776–782. [\[CrossRef\]](#)

30. Wang, D.; Yan, W.; Botte, G.G. Exfoliated nickel hydroxide nanosheets for urea electrolysis. *Electrochem. Commun.* **2011**, *13*, 1135–1138. [\[CrossRef\]](#)
31. Singh, R.K.; Schechter, A. Electrochemical investigation of urea oxidation reaction on  $\beta$  Ni(OH)<sub>2</sub> and Ni/Ni(OH)<sub>2</sub>. *Electrochim. Acta* **2018**, *278*, 405–411. [\[CrossRef\]](#)
32. Kudo, S.; Goto, N.; Sperry, J.; Norinaga, K.; Hayashi, J.I. Production of levoglucosenone and dihydrolevoglucosenone by catalytic reforming of volatiles from cellulose pyrolysis using supported ionic liquid phase. *ACS Sustain. Chem. Eng.* **2017**, *5*, 1132–1140. [\[CrossRef\]](#)
33. Babar, P.; Lokhande, A.; Karade, V.; Pawar, B.; Gang, G.M.; Pawar, S.; Kim, H.J. Bifunctional 2D electrocatalysts of transition metal hydroxide nanosheet arrays for water splitting and urea electrolysis. *ACS Sustain. Chem. Eng.* **2019**, *7*, 10035–10043. [\[CrossRef\]](#)
34. Shen, F.; Jiang, W.; Qian, G.; Chen, W.; Zhang, H.; Luo, L.; Yin, S. Strongly coupled carbon encapsulated Ni-WO<sub>2</sub> hybrids as efficient catalysts for water-to-hydrogen conversion via urea electro-oxidation. *J. Power Sources* **2020**, *458*, 228014. [\[CrossRef\]](#)
35. Xiong, P.; Ao, X.; Chen, J.; Li, J.G.; Lv, L.; Li, Z.; Zondode, M.; Xue, X.; Lan, Y.; Wang, C. Nickel diselenide nanoflakes give superior urea electrocatalytic conversion. *Electrochimica Acta* **2019**, *297*, 833–841. [\[CrossRef\]](#)
36. Gong, M.; Li, Y.; Wang, H.; Liang, Y.; Wu, J.Z.; Zhou, J.; Wang, J.; Regier, T.; Wei, F.; Dai, H. An advanced Ni-Fe layered double hydroxide electrocatalyst for water oxidation. *J. Am. Chem. Soc.* **2013**, *135*, 8452–8455. [\[CrossRef\]](#)
37. Yafarova, L.V.; Chislova, I.V.; Zvereva, I.A.; Kryuchkova, T.A.; Kost, V.V.; Sheshko, T.F. Sol-gel synthesis and investigation of catalysts on the basis of perovskite-type oxides GdMO<sub>3</sub> (M = Fe, Co). *J. Sol-Gel Sci. Technol.* **2019**, *92*, 264–272. [\[CrossRef\]](#)
38. Wu, M.S.; Lin, G.W.; Yang, R.S. Hydrothermal growth of vertically-aligned ordered mesoporous nickel oxide nanosheets on three-dimensional nickel framework for electrocatalytic oxidation of urea in alkaline medium. *J. Power Sources* **2014**, *272*, 711–718. [\[CrossRef\]](#)
39. Yang, P.; Yuan, X.; Hu, H.; Liu, Y.; Zheng, H.; Yang, D.; Li, Y. Solvothermal synthesis of alloyed PtNi colloidal nanocrystal clusters (CNCs) with enhanced catalytic activity for methanol oxidation. *Adv. Funct. Mater.* **2018**, *28*, 1704774. [\[CrossRef\]](#)
40. Premnath, K.; Arunachalam, P.; Amer, M.S.; Madhavan, J.; Al-Mayouf, A.M. Hydrothermally synthesized nickel molybdenum selenide composites as cost-effective and efficient trifunctional electrocatalysts for water splitting reactions. *Int. J. Hydrogen Energy* **2019**, *44*, 22796–22805. [\[CrossRef\]](#)
41. Pang, H.; Wei, C.; Li, X.; Li, G.; Li, S.; Chen, J.; Zhang, J. Microwave-assisted synthesis of NiS<sub>2</sub> nanostructures for supercapacitors and cocatalytic enhancing photocatalytic H<sub>2</sub> production. *Sci. Rep.* **2014**, *4*, 3577. [\[CrossRef\]](#) [\[PubMed\]](#)
42. Kim, H.; Park, H.; Kim, D.K.; Choi, I.; Kim, S.K. Pulse-electrodeposited nickel phosphide for high-performance proton exchange membrane water electrolysis. *J. Alloys Compd.* **2019**, *785*, 296–304. [\[CrossRef\]](#)
43. Shaddad, M.N.; Arunachalam, P.; Hezam, M.; Al-Mayouf, A.M. Cooperative Catalytic Behavior of SnO<sub>2</sub> and NiWO<sub>4</sub> over BiVO<sub>4</sub> Photoanodes for Enhanced Photoelectrochemical Water Splitting Performance. *Catalysts* **2019**, *9*, 879. [\[CrossRef\]](#)
44. Shaddad, M.N.; Arunachalam, P.; Allothman, A.A.; Beagan, A.M.; Alshawi, M.N.; Al-Mayouf, A.M. Synergetic catalytic behavior of AgNi-OH-Pi nanostructures on Zr: BiVO<sub>4</sub> photoanode for improved stability and photoelectrochemical water splitting performance. *J. Catal.* **2019**, *371*, 10–19. [\[CrossRef\]](#)
45. Torabinejad, V.; Aliofkhaezai, M.; Assareh, S.; Allahyarzadeh, M.H.; Rouhaghdam, A.S. Electrodeposition of Ni-Fe alloys, composites, and nano coatings—A review. *J. Alloys Compd.* **2017**, *691*, 841–859. [\[CrossRef\]](#)
46. Hong, B.; Jiang, C.; Wang, X. Texture of electroplated copper film under biaxial stress. *Mater. Trans.* **2006**, *47*, 2299–2301. [\[CrossRef\]](#)
47. Song, Y.; Oh, J.; Park, K. Pt nanostructure electrodes pulse electrodeposited in PVP for electrochemical power sources. *Nanotechnology* **2008**, *19*, 355602. [\[CrossRef\]](#)
48. Wang, D.; Yan, W.; Vijapur, S.H.; Botte, G.G. Enhanced electrocatalytic oxidation of urea based on nickel hydroxide nanoribbons. *J. Power Sources* **2012**, *217*, 498–502. [\[CrossRef\]](#)
49. Ye, K.; Zhang, D.; Guo, F.; Cheng, K.; Wang, G.; Cao, D. Highly porous nickel@ carbon sponge as a novel type of three-dimensional anode with low cost for high catalytic performance of urea electro-oxidation in alkaline medium. *J. Power Sources* **2015**, *283*, 408–415. [\[CrossRef\]](#)
50. Duan, T.; Chen, Y.; Wen, Q.; Duan, Y. Enhanced electrocatalytic activity of nano-TiN composited Ti/Sb-SnO<sub>2</sub> electrode fabricated by pulse electrodeposition for methylene blue decolorization. *RSC Adv.* **2014**, *4*, 57463–57475. [\[CrossRef\]](#)
51. Bourbos, E.; Karantonis, A.; Sygellou, L.; Paspaliaris, I.; Panias, D. Study of Nd Electrodeposition from the Aprotic Organic Solvent Dimethyl Sulfoxide. *Metals* **2018**, *8*, 803. [\[CrossRef\]](#)
52. Chen, R.; Xu, D.; Guo, G.; Gui, L. Preparation of Ag<sub>2</sub>Se and Ag<sub>2</sub>Se<sub>1-x</sub>Te<sub>x</sub> nanowires by electrodeposition from DMSO baths. *Electrochem. Commun.* **2003**, *5*, 579–583. [\[CrossRef\]](#)
53. Gan, Q.; Cheng, X.; Chen, J.; Wang, D.; Wang, B.; Tian, J.; Isimjan, T.T.; Yang, X. Temperature effect on crystallinity and chemical states of nickel hydroxide as alternative superior catalyst for urea electrooxidation. *Electrochim. Acta* **2019**, *301*, 47–54. [\[CrossRef\]](#)
54. Bahramian, A.; Eyraud, M.; Vacandio, F.; Hornebecq, V.; Djenizian, T. Single-step electrodeposition of superhydrophobic black NiO thin films. *J. Appl. Electrochem.* **2020**, *49*, 621–629. [\[CrossRef\]](#)
55. Gomez, H.; Riveros, G.; Ramirez, D.; Henriquez, R.; Schrebler, R.; Marotti, R.; Dalchiale, E. Growth and characterization of ZnO nanowire arrays electrodeposited into anodic alumina templates in DMSO solution. *Solid State Electrochem.* **2012**, *16*, 197–204. [\[CrossRef\]](#)
56. Ding, H.; Feng, Y.; Liu, J. Preparation and properties of Ti/SnO<sub>2</sub>-Sb<sub>2</sub>O<sub>5</sub> electrodes by electrodeposition. *Mater. Lett.* **2007**, *61*, 4920–4923. [\[CrossRef\]](#)



57. Watanabe, T. *NANO Plating, Microstructure Control Theory of Plated Film and Data Base of Plated Film Microstructure*; Elsevier Ltd.: Amsterdam, The Netherlands, 2003.
58. Yin, A.J.; Li, J.; Jian, W.; Bennett, A.J.; Xu, J.M. Fabrication of highly ordered metallic nanowire arrays by electrodeposition. *Appl. Phys. Lett.* **2001**, *79*, 1039–1041.
59. Duan, Y.; Chen, Y.; Wen, Q.; Duan, T. Electrodeposition preparation of a cauliflower-like Sb-SnO<sub>2</sub> electrode from DMSO solution for electrochemical dye decolorization. *RSC Adv.* **2016**, *6*, 48043–48048. [\[CrossRef\]](#)
60. Arunachalam, P.; Ghanem, M.A.; Al-Mayouf, A.M.; Al-shalwi, M.; Abd-Elkader, O.H. Microwave assisted synthesis and characterization of Ni/NiO nanoparticles as electrocatalyst for methanol oxidation in alkaline solution. *Mater. Res. Express* **2017**, *4*, 025035. [\[CrossRef\]](#)
61. Arunachalam, P.; Ghanem, M.A.; Al-Mayouf, A.M.; Al-shalwi, M. Enhanced electrocatalytic performance of mesoporous nickel-cobalt oxide electrode for methanol oxidation in alkaline solution. *Mater. Lett.* **2017**, *196*, 365–368.
62. Ghanem, M.A.; Al-Mayouf, A.M.; Singh, J.P.; Abiti, T.; Marken, F. Mesoporous nickel/nickel hydroxide catalyst using liquid crystal template for ethanol oxidation in alkaline solution. *J. Electrochem. Soc.* **2015**, *162*, H453. [\[CrossRef\]](#)
63. Su, Y.-Z.; Xiao, K.; Li, N.; Liu, Z.-Q.; Qiao, S.-Z. Amorphous Ni(OH)<sub>2</sub>@ three-dimensional Ni core-shell nanostructures for high capacitance pseudocapacitors and asymmetric supercapacitors. *J. Mater. Chem. A* **2014**, *2*, 13845–13853. [\[CrossRef\]](#)
64. Liu, Z.Q.; Xiao, K.; Xu, Q.Z.; Li, N.; Su, Y.Z.; Wang, H.J.; Chen, S. Fabrication of hierarchical flower-like super-structures consisting of porous NiCo<sub>2</sub>O<sub>4</sub> nanosheets and their electrochemical and magnetic properties. *RSC Adv.* **2013**, *4*, 4372–4380. [\[CrossRef\]](#)
65. Liu, Z.Q.; Xu, Q.Z.; Wang, J.Y.; Li, N.; Guo, S.H.; Su, Y.Z.; Wang, H.J.; Zhang, J.H.; Chen, S. Facile hydrothermal synthesis of urchin-like NiCo<sub>2</sub>O<sub>4</sub> spheres as efficient electrocatalysts for oxygen reduction reaction. *Int. J. Hydrogen Energy* **2013**, *38*, 6657–6662. [\[CrossRef\]](#)
66. Rahim, M.A.; Hameed, R.A.; Khalil, M.W. Nickel as a catalyst for the electro-oxidation of methanol in alkaline medium. *J. Power Sources* **2004**, *134*, 160–169. [\[CrossRef\]](#)
67. Jafarian, M.; Babaei, M.; Gobal, F.; Mahjani, M.G. Electro-oxidation of alcohols on nickel dispersed in poly-o-aminophenol modified graphite electrode. *J. Electroanal. Chem.* **2011**, *652*, 8–12. [\[CrossRef\]](#)
68. Hosseini, S.; Abbasi, A.; Uginet, L.O.; Haustraete, N.; Praserttham, S.; Yonezawa, T.; Kheawhom, S. The influence of dimethyl sulfoxide as electrolyte additive on anodic dissolution of alkaline zinc-air flow battery. *Sci. Rep.* **2019**, *9*, 1–12.
69. Vedharathinam, V.; Botte, G.G. Direct evidence of the mechanism for the electro-oxidation of urea on Ni(OH)<sub>2</sub> catalyst in alkaline medium. *Electrochim. Acta* **2013**, *108*, 660–665.
70. Danaee, I.; Jafarian, M.; Forouzandeh, F.; Gobal, F.; Mahjani, M.G. Electrocatalytic oxidation of methanol on Ni and NiCu alloy modified glassy carbon electrode. *Int. J. Hydrogen Energy* **2008**, *33*, 4367–4376.
71. Li, B.; Ai, M.; Xu, Z. Mesoporous β-Ni(OH)<sub>2</sub>: synthesis and enhanced electrochemical performance. *Chem. Commun.* **2010**, *46*, 6267–6269.
72. Yi, Q.; Huang, W.; Yu, W.; Li, L.; Liu, X. Hydrothermal Synthesis of Titanium-Supported Nickel Nanoflakes for Electrochemical Oxidation of Glucose. *Electroanalysis* **2008**, *20*, 2016–2022. [\[CrossRef\]](#)
73. Ding, R.; Qi, L.; Jia, M.; Wang, H. Facile synthesis of mesoporous spinel NiCo<sub>2</sub>O<sub>4</sub> nanostructures as highly efficient electrocatalysts for urea electro-oxidation. *Nanoscale* **2014**, *6*, 1369–1376. [\[CrossRef\]](#) [\[PubMed\]](#)
74. Wang, S.; Chang, J.; Xue, H.; Xing, W.; Feng, L. Catalytic Stability Study of a Pd-Ni<sub>2</sub>P/C Catalyst for Formic Acid Electrooxidation. *ChemElectroChem* **2017**, *4*, 1243–1249. [\[CrossRef\]](#)
75. Xu, Q.; Qian, G.; Yin, S.; Yu, C.; Chen, W.; Yu, T.; Luo, L.; Xia, Y.; Tsiakaras, P. Design and Synthesis of Highly Performing Bifunctional Ni-NiO-MoNi Hybrid Catalysts for Enhanced Urea Oxidation and Hydrogen Evolution Reactions. *ACS Sustain. Chem. Eng.* **2020**, *8*, 7174–7181. [\[CrossRef\]](#)
76. Qian, G.; Chen, J.; Luo, L.; Zhang, H.; Chen, W.; Gao, Z.; Yin, S.; Tsiakaras, P. Novel Bifunctional V<sub>2</sub>O<sub>3</sub> Nanosheets Coupled with N-Doped-Carbon Encapsulated Ni Heterostructure for Enhanced Electrocatalytic Oxidation of Urea-Rich Wastewater. *ACS Appl. Mater. Interfaces* **2020**, *12*, 38061–380619. [\[CrossRef\]](#) [\[PubMed\]](#)
77. Singh, R.K.; Subramanian, P.; Schechter, A. Enhanced urea activity of oxidation on nickel-deposited tin dendrites. *ChemElectroChem* **2017**, *4*, 1037–1043. [\[CrossRef\]](#)
78. Forslund, R.P.; Alexander, C.T.; Abakumov, A.M.; Johnston, K.P.; Stevenson, K.J. Enhanced electrocatalytic activities by substitutional tuning of nickel-based ruddlesden–popper catalysts for the oxidation of urea and small alcohols. *ACS Catal.* **2019**, *9*, 2664–2673.
79. Ghanem, M.A.; Al-Mayouf, A.M.; Singh, J.P.; Arunachalam, P. Concurrent deposition and exfoliation of nickel hydroxide nanoflakes using liquid crystal template and their activity for urea electrooxidation in alkaline medium. *Electrocatalysis* **2017**, *8*, 16–26. [\[CrossRef\]](#)
80. Sharel, P.E.; Liu, D.; Lazenby, R.A.; Sloan, J.; Vidotti, M.; Unwin, P.R.; Macpherson, J.V. Electrodeposition of nickel hydroxide nanoparticles on carbon nanotube electrodes: correlation of particle crystallography with electrocatalytic properties. *J. Phys. Chem. C* **2016**, *120*, 16059–16068.